HPC Everywhere

SC13

2013 Chair
William Gropp
Denver, Colorado

SC13
Denver, CO | 2013

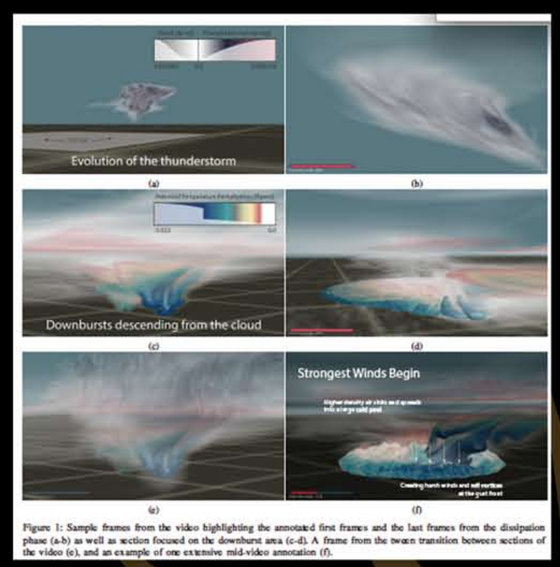

Figure 1: Sample frames from the video highlighting the annotated first frames and the last frames from the dissipation phase (a-b) as well as section focused on the downburst area (c-d). A frame from the tween transition between sections of the video (e), and an example of one extensive mid-video annotation (f).

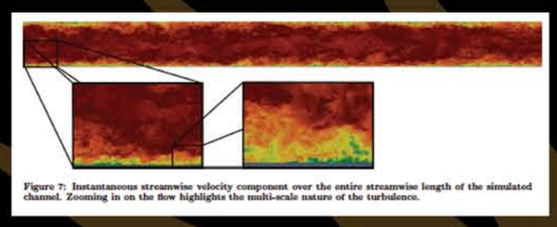

Figure 7: Instantaneous streamwise velocity component over the entire streamwise length of the simulated channel. Zooming in on the flow highlights the multi-scale nature of the turbulence.

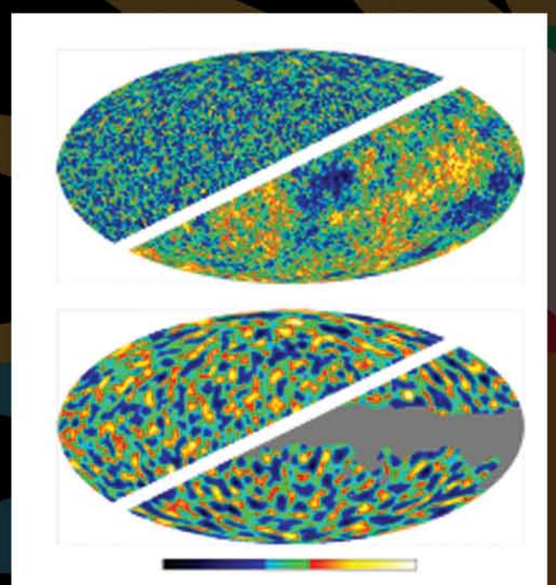

2013

Notable Systems:
- Titan
- Mira
- Sequoia
- Stampede
- Blue Waters
- K-Computer
- Curie
- Tianhe-2

Notable Processors/Architectures:
- Intel Xeon Phi
- Nvidia Kepler
- IBM BlueGene/Q Compute Processor
- Fujitsu Sparc64 IXfx

Noteworthy Architecture Topics:
- Energy management
- Nonvolatile Memory
- Fault Tolerance

Notable Applications:
- Computations on Large Graphs
- Computational Biology

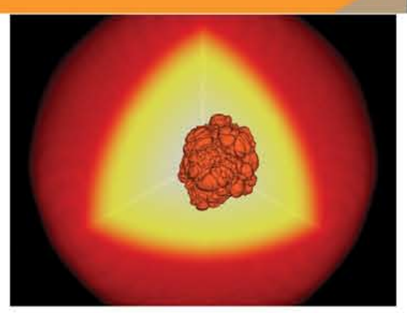

Figure 1. Complex structure of the turbulent thermonuclear flame propagating through the interior of a degenerate white dwarf star during the SN Ia explosion prior to the putative transition to a detonation. Computation is performed on an adaptive mesh with the highest resolution of ~600 m. Diameter of the star is ~4,000 km. The turbulent flame dynamics is captured using a subgrid-scale model intended to reproduce the correct burning rate on the small unresolved scales.

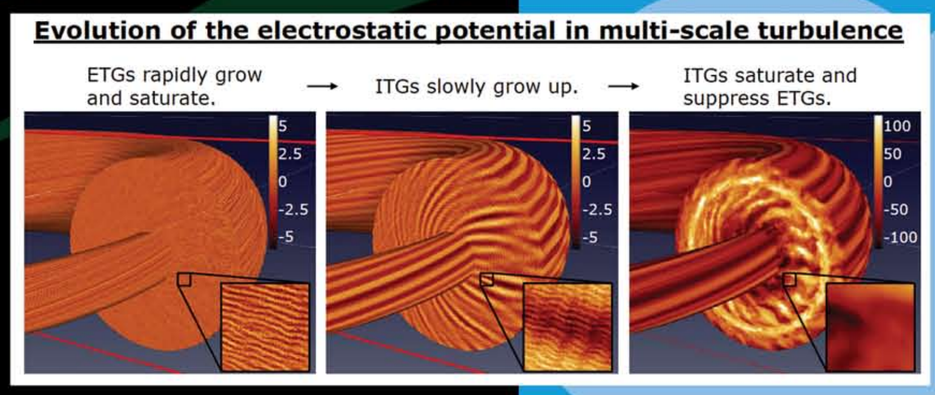

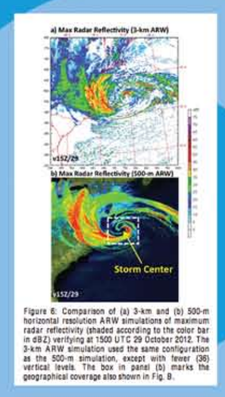

Figure 6: Comparison of (a) 3-km and (b) 500-m horizontal resolution ARW simulations of maximum radar reflectivity (shaded according to the color bar in dBZ) verifying at 1500 UTC 29 October 2012. The 3-km ARW simulation used the same configuration as the 500-m simulation, except with fewer (36) vertical levels. The box in panel (b) marks the geographical coverage also shown in Fig. 8.

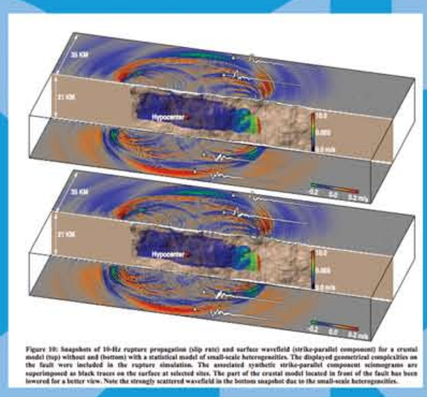

Figure 10: Snapshots of 10-Hz rupture propagation (slip rate) and surface wavefield (strike-parallel component) for a crustal model (top) without and (bottom) with a statistical model of small-scale heterogeneities. The displayed geometrical complexities on the fault were included in the rupture simulation. The associated synthetic strike-parallel component seismograms are superimposed as black traces on the surface at selected sites. The part of the crustal model located in front of the fault has been lowered for a better view. Note the strongly scattered wavefield in the bottom snapshot due to the small-scale heterogeneities.

Denver, CO